2016 American Control Conference (ACC)
Boston Marriott Copley Place
July 6-8, 2016. Boston, MA, USA

Kalman Filter Estimation with Edge Detection-Based Hybrid Sensing

Y. Chen and K. R. Oldham

***Abstract*—A novel sensing and estimation scheme is introduced as an integrated part of a micro-stage based calibration method for a MEMS gyroscope. The proposed sensing scheme combines a periodically updating analog sensor with an event-based threshold sensor. A first derivative of Gaussian filter is applied to the threshold sensor signal to detect threshold crossings. A Kalman filter with the proposed sensing scheme is used to estimate the micro-stage's states. In the measurement update steps, analog sensor measurement is used when a threshold crossings event is not triggered, and the threshold sensor measurement is used when the crossing event is triggered. The impact of detection error of the proposed threshold detection technique on the estimation performance is evaluated with estimation error covariance analysis and simulations.**

I. INTRODUCTION

MEMS gyroscopes are subject to long term gain and bias drift, which can make accurate measurement difficult in many cases [1]. Laboratory calibration methods rely on high accuracy instrumentation, such as rate tables, and an external stimulus needs to be provided [2]. Another calibration approach is to model MEMS sensors' noise and drift with respect to changes in environmental factors, such as temperature, and to compensate for the drift and bias accordingly [3]. However, such a calibration method is limited by sensors' individual properties.

An approach proposed [4], [5] and [6] is to use a piezoelectric micro-stage to approximate some functionality of a rate table, i.e., providing certain external stimulus and measurements to the gyroscope. In such a micro-actuation stage, high accuracy but asynchronous threshold sensor measurements are proposed for use in state estimation to assist noisy analog sensor measurement, as the latter are highly vulnerable themselves to bias and environmental effects. Figure 1 depicts the basic concept of such type of threshold sensor. In the side-view (upper left), the piezoelectric micro-stage contains a rotors and a stator. Electrodes are attached to the inner surfaces of the rotor and stator to create capacitance that varies with respect to the relative position of the rotor and stator. The position where rotor and stator fully overlap generates the largest capacitance, and this defines the threshold angle (lower left).

To implement the proposed estimation technique, one key point is to overwrite noisy analog sensor measurement with more accurate but infrequent threshold sensor measurement whenever such an event is triggered. Such a sampling strategy resembles so-called event-based sampling. The strategies and corresponding estimation methods have been widely explored in last decades. Nguyen and Suh [7] and Sijs and Lazar [8] studied the situation where measurements are only transmitted then the change of signal or the change of the integration of the signal exceeds certain threshold value. In [9] and [10], a measurement is transmitted as binary digits to indicate if the measurement surpasses certain threshold value.

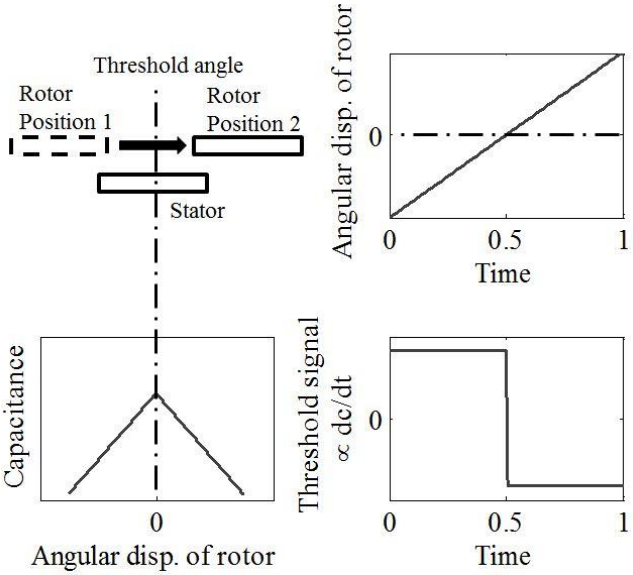

Figure 1. Principles of threshold sensing with parallel electrodes: Schematic (upper left); capacitance vs. angular displacement (lower left)'; angular displacement vs. time (upper right); and threshold signal vs. time (lower right).

Even with threshold sensing, signals being measured are almost always subject to a certain amount of noise and bias, and this can affect the detection accuracy and result in deteriorated estimation performance. So detecting whether the signal reaches certain threshold value is non-trivial. Furthermore, how the detection error affects estimation performance and how to minimize such impact has practical significance, but these issues have been much less reported. Rather, most previous work assumes the events are readily available with perfect knowledge of when threshold crossing events occurs.

To address this issue, we first adopt an edge detection algorithm widely used in the imaging processing and computer vision field [11] to detect if threshold sensor's measurement reaches threshold value. A Kalman filter estimation is then implemented with the hybrid sensing scheme. We also derive a method to evaluate how such a detection algorithm affects estimation performance. Simulation results are presented for validation.

This paper is organized as follows: Section II provides the model of the dynamics of the MEMS device and Kalman filter state estimation. Section III introduces the threshold

sensing mechanism, threshold crossing event detection algorithm and implementation. Section IV provides the Kalman filter state estimation with hybrid sensing scheme and derivation for error covariance. Finally, Section V and VI provide simulation results and conclusions.

II. System Model and Baseline Kalman Filter

In this section, the dynamics of the piezoelectric stage are introduced, along with the associated Kalman filter using only analog sensor measurements.

A. System Dynamics of piezoelectric stage

During the calibration process, the piezoelectric stage, together with the MEMS inertial measurement unit (IMU) as the payload, tilts along a specified axis, and both analog and threshold sensor measurements are provided by the stage for the purpose of gyroscope calibration [4]. The dynamics of the integrated system is assumed to be a linear, time-invariant second order system dynamics for the purpose of this discussion, with the system being described as

$$\dot{x} = A_c x + B_c u + w$$
$$y = C_c x + v \tag{1}$$

where A_c, B_c, C_c are $\mathbb{R}^{n_x \times n_x}, \mathbb{R}^{n_x \times n_u}, \mathbb{R}^{n_y \times n_x}$ matrices respectively, x is the system states (angular displacement and angular velocity), y is the analog sensor measurement provided by piezoelectric stage and w and v are zero-mean, normally distributed process and measurement noise respectively. For the sake of analysis and implementation, the system dynamics, as well as the analog sensor measurement, are discretized at sampling rate T:

$$x_k = Ax_{k-1} + Bu_{k-1} + w_{k-1}$$
$$y_k = Cx_k + v_k \tag{2}$$

where x_k, u_k, y_k are discretized states, system input and analog sensor output respectively, A, B, C are $\mathbb{R}^{n_x \times n_x}, \mathbb{R}^{n_x \times n_u}, \mathbb{R}^{n_y \times n_x}$ matrices respectively. w_k and v_k are discretized process noise and measurement noise respectively, which are assumed to have zero-mean and normal distribution, with variance matrices of Q and R with dimension of $\mathbb{R}^{n_x \times n_x}$.

B. Kalman Filter with Analog Sensor

A Kalman filter with only analog sensor measurement available is defined as a baseline estimation scheme. The following equation shows the states estimation procedures.

Prediction updates:

$$\hat{x}_k^- = A\hat{x}_{k-1}^- + Bu_{k-1}$$
$$P_k = AZ_{k-1}A^T + Q \tag{3}$$

Measurement updates:

$$K_k = P_k C^T (CP_k C^T + R)^{-1}$$
$$\hat{x}_k = \hat{x}_k^- + K_k(y_k - C\hat{x}_k^-)$$
$$Z_k = (I - K_k C)P_k \tag{4}$$

where P_k is the a-priori error covariance matrix with dimension of $\mathbb{R}^{n_x \times n_x}$, Z_k is the a-posteriori error covariance matrix with dimension of $\mathbb{R}^{n_x \times n_x}$, $\hat{x}_k^-$ is the a-priori estimated state, $\hat{x}_k$ is the a-posteriori error covariance and K_k is the optimal Kalman filter gain matrix with dimension of $\mathbb{R}^{n_x \times n_y}$.

III. Threshold Sensor and Detection

This section describes the threshold sensor mechanism, threshold-crossing event detection algorithm as well as the method to quantify the variance of detection error.

A. Threshold Sensor Mechanism

The threshold sensor is designed to indicate when the system states cross pre-defined threshold values (specific angles in the context of this paper). The hardware of such sensor includes several sets of specifically designed and positioned capacitive sensors (Figure 1) and a sensing circuitry. The sensing circuitry consists of a feedback type ammeter [12] to convert the sensing charge into voltage output.

$$G_{th} = V_b R_s \frac{dC_{th}}{dt} \tag{5}$$

where V_b is the constant bias voltage applied to the capacitors. dC_{th}/dt is the change of capacitance w.r.t. time, R_s, is the shunt resistance and G_{th} is the voltage output.

It is assumed that the threshold signal is subject to additive white Gaussian noise v_{th} with variance of R_{th} and a possible constant, unknown bias b_{th}, as noted in the equation below.

$$y_{th} = G_{th} + v_{th} + b_{th} \tag{6}$$

It is worth pointing out that the threshold value is defined when the sensing electrodes are fabricated, depending on the application, it can be multiple sets for different threshold value measurement. For the sake of this study, we assume one set threshold sensor in the given sensing scheme and denote the threshold value to be M.

B. Threshold-crossing event detection

As shown in the upper and middle subplot of Figure 2, as the angular displacement of the piezoelectric stage crosses the threshold value, the value of the clean threshold signal changes rapidly from positive to negative (notice that the sign change of angular velocity at the bottom of the sinusoidal waves also result into threshold-crossings, but the slopes are less sharp). However, due to the corruption of noise and bias, the number of apparent crossing events can increase significantly, making it difficult to identify the true crossing. Without knowing the timing of right crossing event accurately, the calibration accuracy will be undermined, the timing of the threshold angle crossing will not be known. To resolve this issue, a threshold crossing detection method that is robust to noise and bias is needed.

To detect the threshold crossing, a first derivative of Gaussian filter has been selected for optimal edge detection and localization performance [11]. The filter is extensively used in image processing and computer vision field to detect edges within pictures [12], detectable as sudden changes in

pixel values. We denote f is the first derivative of Gaussian filter with filter width of $2w$, and the filtered response is defined as

$$D = \int_{-w}^{w} y_{th}(-x)f(x)dx \tag{7}$$

The benefit of the such filter is that by simplify examining the local maxima of the filtered signal, one can pick the location threshold single crossing despite certain amount of noise and bias, as depicted in the lower subplot of Figure 2.

C. Detection error and its variance

Due to the existence of noise in the threshold signal, the detection of threshold crossing is not always accurate and the true crossing and detected crossing will have certain localization error. Such error in determining the true crossing time, noted as e_t, will result in error in the state estimation process. In order to evaluate its impact to the state estimation performance, the statistical attributes of detection timing error as relevant to estimator performance are derived using the following equations. First, threshold sensor measurement error at the true crossing timing, e_d is approximated as

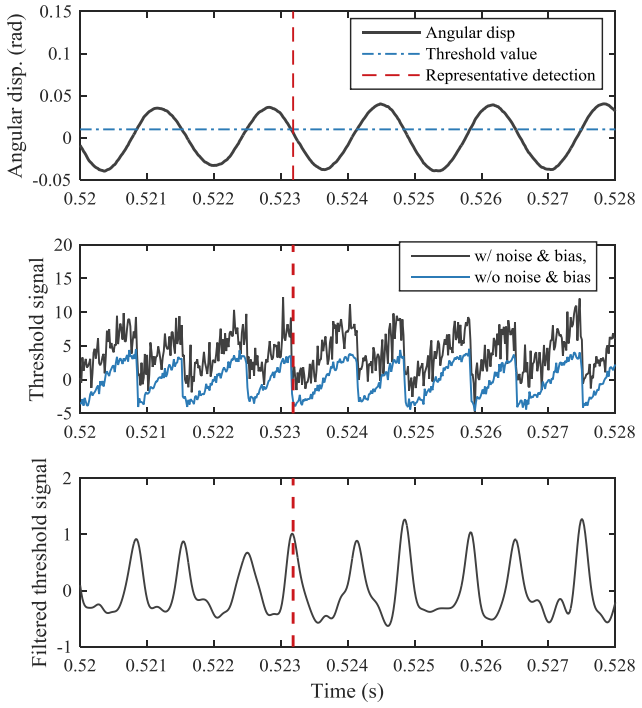

Figure 2 Signals relevant to threshold crossing detection: Angular displacement (upper); threshold sensor signal (middle); and filtered threshold sensor signal (lower) vs. time. The local maxima of filtered response indicate threshold signal crossing.

$$e_d \approx \dot{\hat{x}} e_t \tag{8}$$

where $\dot{\hat{x}}$ is the estimated derivative of states. The variance of e_d, R_d can then be computed as

$$R_d = \dot{\hat{x}}^2 R_t \tag{9}$$

where R_t is the variance of e_t. By definition,

$$R_t = E[e_t^2] - E[e_t]^2 \tag{10}$$

and from [11], it is known that

$$E[e_t^2] \approx \frac{R_{th}\int_{-w}^{w}\dot{f}(\tau)^2 d\tau}{\left[\int_{-w}^{w}\dot{f}(\tau)\dot{G}_{th}(-\tau)d\tau\right]^2} \approx \frac{R_{th}\int_{-w}^{w}\dot{f}(\tau)^2 d\tau}{\left[\int_{-w}^{w}\dot{f}(\tau)\dot{y}_{th}(-\tau)d\tau\right]^2} \tag{11}$$

where R_{th} is the variance of zero mean Gaussian noise v_{th}. Since v_{th} is has zero mean value, we know that

$$E[e_t] = E\left[\frac{-\int_{-w}^{w} v_{th}(e_t - x)\dot{f}(x)dx}{\int_{-w}^{w}\dot{G}_{th}(-x)\dot{f}(x)dx}\right] = 0. \tag{12}$$

Notice that $\dot{G}_{th}$replaces $\dot{y}_{th}$ in (11) and (12) due to the fact that $\dot{G}_{th}$ is not available in practical implementation reality. While this can potentially introduce error, simulation results suggest that this approximation does not have a significant impact on estimation performance.

D. Threshold detection implementation in discretized time domain

The threshold detection is implemented in a discretized time domain. In this paper, the threshold sensor's sampling rate chosen to be the same as the analog sampling rate, *T*. However, it is possible set them to be different to obtain potentially better estimation performance and take advantage of relative simplicity of threshold sensing hardware compared to analog capacitive sensing circuitry.

In discretized time domain for, the filtered response of threshold sensing single D_k is denoted as

$$D_k = \sum_{j=-w}^{w} y_{th\_j} f_{k-j+1} \tag{13}$$

where y_{th_k} and f_k are the discretized threshold sensor measurement and derivative of Gaussian filter, respectively. The discretized threshold sensor measurement error at k_{th} step, e_{d_k} is approximated as

$$e_{d\_k} \approx \dot{\hat{x}}_{k-1} e_{t\_k} \tag{14}$$

where $\dot{\hat{x}}_{k-1}$ is the estimated derivative of states at the previous step. Therefore the variance of e_{d_k}, R_{d_k} is computed as

$$R_{d\_k} = \dot{\hat{x}}_{k-1} R_{t\_k} \dot{\hat{x}}_{k-1}^T \tag{15}$$

and the variance ofe_{t_k}, R_{t_k} is calculated as

$$R_{t\_k} = \frac{R_{th\_d}\sum_{j=-w}^{w}\dot{f}_{k-j+1}^2}{\left[\sum_{j=-w}^{w}\dot{G}_{th\_j}\dot{f}_{k-j+1}\right]^2} \tag{16}$$

where R_{th_d} is the variance of threshold sensor measurement noise in discretized time domain.

IV. Kalman Filter with Hybrid Sensing Scheme and Estimation Performance

The estimation scheme was first introduced in work done by Edamana, et al. [5], in which the timing of threshold crossing events is perfectly known without any uncertainty. However, this is not true in most cases. This section thus characterizes such uncertainty on the threshold crossing event detection process and introduces it into the Kalman filter state estimation process, to quantify the estimation performance with the addition of threshold signal.

A. Kalman Filter with Hybrid Sensing Scheme

When equipped with both an analog sensor and threshold sensor, the procedures for the Kalman filter update with measurement changes compared to that in Section II.B. If in current step the threshold crossing event detection result is negative, then all the estimation steps remains the same as standard Kalman filter estimation with analog sensor only, as shown in equations (3) and (4). However, if the threshold crossing event detection in current step is positive, obtained from the detection scheme in Section III, the optimal Kalman gain matrix, the a-posterior state estimate and estimate covariance matrix become

$$K_{th\_k} = P_k C^T (C P_k C^T + R_{d\_k})^{-1}$$
$$\hat{x}_k = \hat{x}_k^- + K_{th\_k}(CM - C\hat{x}_k^-)$$
$$Z_k = \left(I - K_{th\_k} C\right) P_k \quad (17)$$

where K_{th_k} is the optimal Kalman filter gain given threshold sensor measurement and M is the theoretical threshold value pre-defined by capacitive sensor design.

B. Derivations of State Estimation Error Covariance

To evaluate the effectiveness of the Kalman filter estimation combining the normal analog sensor and the threshold sensor scheme, the total a-posterior state estimation error covariance with hybrid sensing scheme at k_{th} step, denoted as Z_{tot_k} is derived as:

$$Z_{tot\_k} = Z_{pos\_k} P_{pos\_k} + Z_{neg\_k} P_{neg\_k} \quad (18)$$

where Z_{pos_k} is the state estimation error covariance with positive detection results at k_{th} step, it is computed as

$$Z_{pos\_k} = E[(x_k - \hat{x}_k)(x_k - \hat{x}_k)^T | x_k = M] P_{pos\_k} \quad (19)$$

where P_{pos} is the probability of the system states cross threshold value M at k_{th} step. Similarly, the state estimation error covariance with negative detection results at k_{th} step is denoted as Z_{neg_k}, and it is computed as

$$Z_{neg\_k} = E[(x_k - \hat{x}_k)(x_k - \hat{x}_k)^T | x_k \neq M] P_{neg\_k} \quad (20)$$

where P_{neg} is the probability of the system states not cross threshold value M at k_{th} step, and

$$P_{neg} = 1 - P_{pos} \quad (21)$$

From (4) and (17) we know that

$$E[(x_k - \hat{x}_k)(x_k - \hat{x}_k)^T | x_k \neq M] = (I - K_k C) P_k \quad (22)$$

$$E[(x_k - \hat{x}_k)(x_k - \hat{x}_k)^T | x_k = M] =$$
$$\left(I - K_{th\_k} C\right) P_k \left(I - K_{th\_k} C\right)^T - K_{th\_k} e_{d\_k} K_{th\_k}^T \quad (23)$$

In order to compute P_{pos}, the probability mass function (PMF) of system state in the discretized time domain is modeled as a Gaussian distribution with a mean of the a-posterior state estimation and a variance of the a-posterior error covariance [13], i.e.,

$$f_{x_k} \sim \mathcal{N}(\hat{x}_k, Z_k) \quad (24)$$

then we can compute P_{pos_k} by summing the values of the PMF in the vicinity of threshold value M.

V. Simulation Results

This section describes simulation results for the proposed estimator. The main focus is to explore the Kalman filter estimation performance with each sensing scheme, and the impact of threshold crossing event detection performance to the estimation results.

A. Threshold crossing detection performance

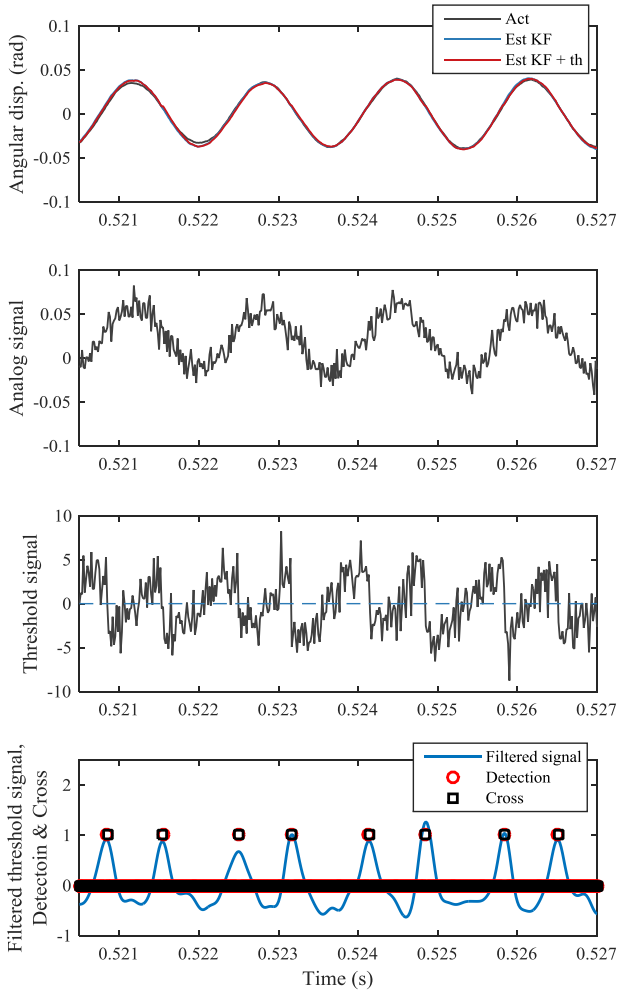

Figure 3 Angular position, analog sensor signal, threshold sensor signal, filtered threshold sensor signal vs. time.

The simulation scheme is coded using Matlab software with discretized sampling rate of 60 kHz. In the simulation, the dynamic system is set to have damping ratio of 0.05 and resonant frequency of 500 Hz. The input is defined as 600 Hz sinusoidal excitation, which produces angular velocities in the physical stage comparable in magnitude to a sample gyroscope maximum range. The sampling rate is 60 kHz for both threshold and analog sensor. To give moderate disturbance and measurement noise, the variance of the process noise is chosen to be 10^{-7}, and measurement noise for analog sensor and threshold sensor are chosen 9.24×10^{-5} and 2.76 respectively. The threshold angle is defined at 0.01 rad. The total width of the derivative of Gaussian filter is chosen to be 49 samples (half of sample numbers of one

period) and the variance for the Gaussian distribution is chosen to be 5 after optimization of detection result. 600 periods of sinusoidal excitation are input to the system and the last 500 periods of the simulation results are taken for analysis to avoid the impact of transient system response.

The angular positon of gyroscope actuator, analog sensor signal, threshold sensor signal and filtered threshold sensor signal vs time is depicted in Figure 3. Subplot (3) and (4) demonstrates that despite the existence of bias and noise, the detected threshold crossing matches the true threshold crossing with good accuracy.

Figure 4 (upper) shows the detected and actual threshold crossing events within each period. During each period the angular displacement of the stage crosses the threshold angle twice, once near sampling location index 55, and once near 90. Figure 4 (lower) shows the detection error distribution in terms of sampling steps. From the figure we can see that the mean of the detection error is about zero, and detection errors of more than one time step are rare.

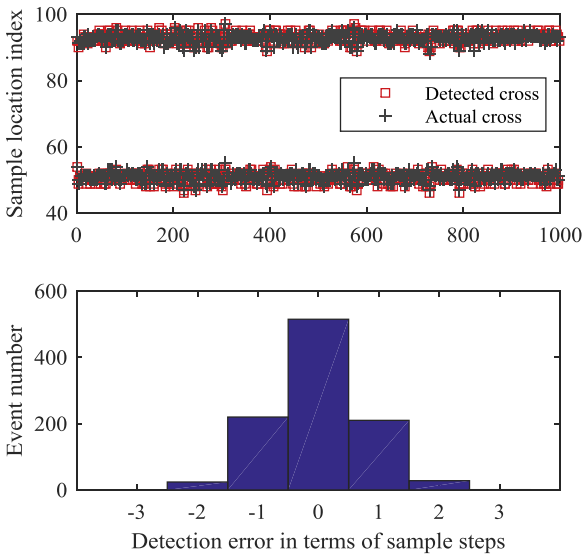

Figure 4 Detected and actual threshold crossing event in each corresponding period shows the threshold crossing events happens near sampling location index of 55 and 90 (upper) and detection error distribution in terms of sampling steps shows the of the detection error is normally distributed with zero mean (lower).

B. Estimation performance

As the goal of the Kalman filter is to minimize the a-posteriori estimate error covariance, it is proper to evaluate the observer's performance by comparing the variance of the state estimation error throughout the operating period, i.e., the diagonal elements of matrix of $E[(x_k - \hat{x}_k)(x_k - \hat{x}_k)^T]$. In particular, for gyroscope calibration, variance in velocity estimates is a major source of calibration error. For the purpose of comparison in this paper, new metrics are defined by extending the definition show in equations (4) and (18). Two theoretical state estimation error variances, $\bar{Z}_{theo}$ and $\bar{Z}_{theo,tot}$ are defined by averaging the diagonal elements of the a-posteriori error covariance matrices generated during the recursive estimation steps over steady state periods. Two simulated state estimation error variance, $\bar{Z}_{sim}$, $\bar{Z}_{sim,tot}$ are obtained by computing the variance of the estimation error over the steady state periods. $\bar{Z}_{theo}$ and $\bar{Z}_{sim}$ are for cases with Kalman filter with analog sensing scheme, $\bar{Z}_{theo,tot}$ and $\bar{Z}_{sim,tot}$ are for Kalman filter with hybrid sensing scheme.

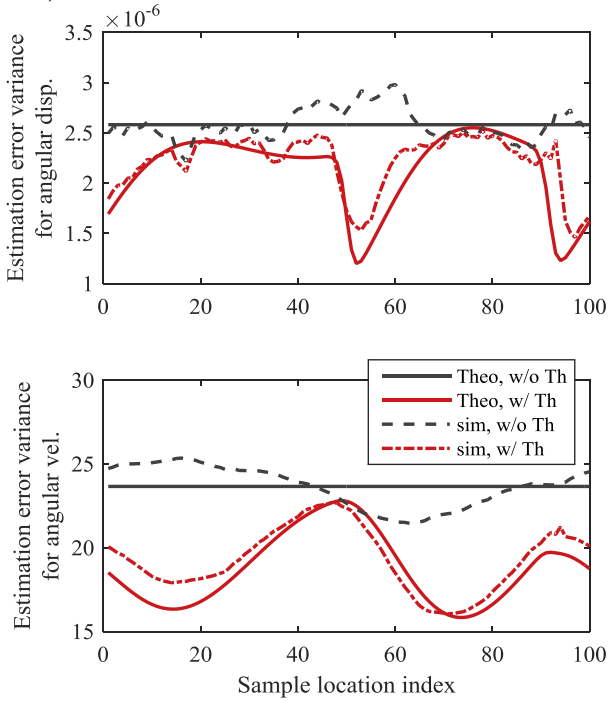

Figure 5 Comparison of error covariance of angular position.

For the purpose of calibration of gyroscope, it is more beneficial to reduce the estimation error by large amount at certain sampling location rather reduce the estimation error over all sampling location by small amount, therefore it more interesting to analyze on the sampling location has best estimation error variance reduction. We hereby define the best reduction rate of state estimation error variance η_B as following:

$$\eta_B = \bar{Z}_{sim,tot}(k_{min}) - \bar{Z}_{sim}(k_{min})/\bar{Z}_{sim}(k_{min}) \quad (25)$$

where k_{min} is the sampling location indicates the minimum estimation error variance for $\bar{Z}_{sim,tot}$.The comparison of the estimation error variances for angular displacement (upper) and angular velocity (lower) are depicted in Figure 5. The locations of the two dips of the estimation error variances of angular displacement with the threshold sensor (red solid and dashed lines) show the reductions of the state estimation error variance that coincide with the average detected threshold event crossing locations. The best reduction rate of state estimation variance, η_B for angular displacement is 43.7% (k_{min}= 97), and the η_B for angular velocity is 27.1% (k_{min} = 71). This shows with the effect of the more accurate threshold sensor measurements for the Kalman Filter to utilize, as the state estimation error variances are reduced. The velocity variance also decreases when provided with more accurate measurements.

Parameter sweeps have been done to investigate the impact of the properties of threshold sensors to the estimator's performance. Both threshold sensor noise variance and the threshold location were varied as tabulated

in Table 1. The η_B calculated from sweeping results are shown in Figure 6. The lowest average state estimation error variance w/ hybrid sensing was found and compared to the average state estimation error variance at same location w/ the baseline estimator.

Table 1. Summary of representative sweeping parameters of threshold sensor. For sweep (a), the threshold location is set to be 0.02 rad, for sweep (b), the threshold sensor noise variance is set to be 1.84×10^{-4}.

Swept Parameter	**Value**				
(a) R_{th_d} $(\times 10^{-4})$	0.92	1.84	2.76	3.68	4.60
(b) M (rad)	0.00	0.01	0.02	0.03	0.04

As show in Figure 6, increasing threshold sensor noise reduces the improvement of state estimation error variance. This is because increasing threshold sensor noise will increase threshold crossing detection error. As a consequence, the advantages of having precise knowledge of certain angular displacements brought by threshold sensor diminish.

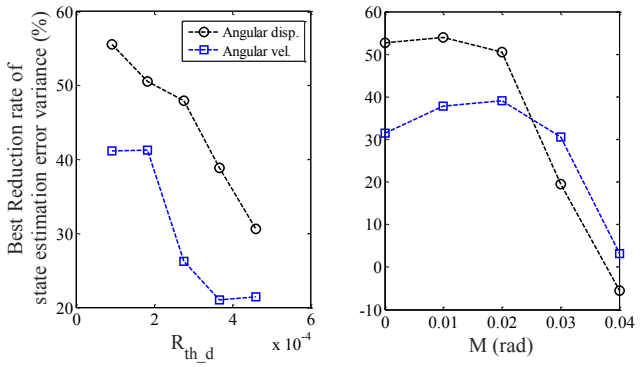

Figure 6 Reduction rate of state estimation error variance in threshold sensor noise variance sweep (left) and threshold location sweep (right).

The threshold location sweep suggests that as the threshold location moves further away from the zero rad position, the best reduction will decrease. This is because the threshold crossing angular velocity of the stage is slower when the threshold location is far away from the neutral stage position; the slower velocity therefore reduces the slope of the threshold crossing signal and increases the detection error, result into worse estimation performance.

VI. Conclusion

In this paper, a novel hybrid sensing and estimation scheme is introduced for a piezoelectric micro-actuator intended for gyroscope calibration. The sensing scheme incorporates a periodically updating analog sensor and an event-based threshold sensor having higher accuracy at a pre-defined threshold value. A derivative of Gaussian filter is adopted in assisting detecting threshold crossing event in the presence of threshold sensor noise and bias. To estimate the gyroscope states, a Kalman filter is applied with the above hybrid sensing scheme. The impact of detection error to the estimation performance has been evaluated in terms of state estimation error variance, which is commonly neglected in estimation with comparable asynchronous sensing events by previous researchers. Simulation results shows that states estimation error covariance predictions derived from statistical behavior of the derivative of Gaussian filter are effective in predicting the performance of Kalman filter with hybrid sensing scheme. As demonstrated, the error variance of states estimation has been reduced by 43.7 % around threshold location. And parametric sweeps shows such the estimation performance is improved most significantly when threshold sensing features low noise and threshold crossings occur at high angular velocity.

Acknowledgment

The authors thank Dr. E.E. Aktakka and Dr. Biju Edamana for information on representative piezoelectric actuator modeling and properties.

References

[1] O. J. Woodman, "An introduction to inertial navigation," University of Cambridge, Computer Laboratory, Cambridge, 2007.

[2] J. K. Bekkeng, "Calibration of a novel MEMS inertial reference unit," *IEEE Transactions on Instrumentation and Measurement,* vol. 58, no. 6, pp. 1967 - 1974, 2008.

[3] D. Xia, S. Chen, S. Wang and H. Li, "Temperature effects and compensation-control methods," *Sensors,* vol. 9, no. 10, pp. 8349 - 8376, 2009.

[4] E. E. Aktakka, J.-K. Woo, D. Egert, R. J. M. Gordenker and K. Najafi, "A microactuation and sensing platform with active lockdown for in situ calibration of scale factor drifts in dual-axis gyroscopes," *IEEE/ASME Transactions on Mechatronics,* vol. 20, no. 2, pp. 934 - 943, 2015.

[5] B. Edamana, Y. Chen, D. Slavin, E. E. Akatakka and K. R. Oldham, "Estimation with threshold sensing for gyroscope calibration using a piezoelectric microstage," *IEEE Transactions on Control Systems Technology,* vol. 23, no. 5, pp. 1943 - 1951, 2015.

[6] J. Qu and K. R. Oldham, "Position estimation for a capacitively-sensed magnetoelastic rotary microstage using an extended Kalman smoother," in *2014 American Control Conference (ACC)*, Portland, 2014.

[7] V. H. Nguyen and Y. S. Suh, "Improving estimation performance in networked control systems applying the send-on-delta transmission method," *Sensors,* vol. 7, no. 10, pp. 2128 - 2138, 2007.

[8] J. Sijs and M. Lazar, "Event based state estimation with time synchronous updates," *IEEE Transactions on Automatic Control,* vol. 57, no. 10, pp. 2650 - 2655, 2012.

[9] T. Henningsson and K. J. Astrom, "Log-concave Observers," in *Mathematical Theory of Networks and Systems*, Kyoto, 2006.

[10] K. J. Astrom, "Event based control," in *Analysis and Design of Nonlinear Control System*, Berlin, Springer Berlin Heidelberg, 2008, pp. 127 - 147.

[11] J. Canny, "A computational approach to edge detection," *IEEE Transactions on Pattern Analysis and Machine Intelligence,* Vols. PAMI - 8, no. 6, pp. 679 - 698, 1986.

[12] M. Basu, "Gaussian-based edge-detection methods-a survey," *IEEE Transactions on Systems, Man and Cybernetics - Part C: pplications and Reviews,* vol. 32, no. 3, pp. 252 - 260, 2002.

[13] R. G. Brown and P. Y. C. Hwang, "Chapter 4: Discrete Kalman filter basics," in *Introduction to random signals and applied Kalman filtering: with MATLAB exercises.*, Hoboken, John Wiley & Sons, 2012.